Co-published by
Institute of Fluid-Flow Machinery
Polish Academy of Sciences
Committee on Thermodynamics and Combustion
Polish Academy of Sciences

http://www.imp.gda.pl/archives-of-thermodynamics/

Three-dimensional modelling of combustion and emissions characteristics in direct-injection diesel engines using detailed chemistry based on the SAGE combustion model

Lamia Medjahed[a], Hamza Bousbaa[b*], Mohammed Benramdane[a], Bouchra Nor El Houda Hagani[b]

[a]Mechanical Department, Technology Faculty, University of Tlemcen, ETAP Laboratory, Algeria
[b]National Polytechnic school Maurice Audin, Mechanical Department, LTE Laboratory, BP 1523 El Menaouer, 31000-Oran, Algeria
*Corresponding author email: hamza.bousbaa@enp-oran.dz

Received: 07.10.2025; revised: 03.05.2026; accepted: 12.05.2026

Abstract

This study employed a three-dimensional CFD model with integrated chemical kinetics using CONVERGE CFD software. We used a detailed mechanism of 42 species and 167 reactions and compared its predictions with a reduced 77-species mechanism developed by Liu and Zhang (2023), both tailored for n-heptane oxidation. Validation of diesel-injection combustion was carried out by comparing the model results with experimental engine data. Numerical simulations were conducted on an MKDIR 620-145 engine at 1400 rpm and 50% load. The chosen models reproduced the mean in-cylinder pressure accurately, with deviations below 4.7%. Analysis of species and thermal fields revealed that key intermediate species emerge near 930 K, where H_2O_2 concentrations become sufficient to trigger auto-ignition and the heat release rate reaches its peak. At higher temperatures (around 1300 K), OH and CO concentrations are notably elevated. Soot production is initiated early in combustion and is dominated by diffusion processes; the peak net soot mass was 3.25×10^{-7} kg at 18° before the top dead centre. Throughout combustion, CO_2, H_2O and hydrocarbon concentrations increase markedly while O_2 is consumed, with CO_2 and H_2O rising rapidly during both premixed and diffusion combustion phases. NO_x formation closely follows the temperature history, approaching a saturation level near 1.1×10^{-4} kg under the studied conditions. Overall, the results indicate that the employed reaction mechanisms capture the temporal evolution of combustion, species formation, soot production and emission trends with good fidelity, supporting their suitability for studying fuel behaviour and emissions in diesel engine environments.

Keywords: CONVERGE CFD software; Diesel engine; Modelling; Chemistry approach; Combustion

Vol. 47(2026), No. 2, 59–68; doi: 10.24425/ather.2026.158681

Cite this manuscript as: Medjahed, L., Bousbaa, H., Benramdane, M., & Hagani, B.N.E.H. (2026). Three-dimensional modelling of combustion and emissions characteristics in direct-injection diesel engines using detailed chemistry based on the SAGE combustion model. *Archives of Thermodynamics*, 47(2), 59−68.

1. Introduction

As the source of energy, propulsion and power, internal combustion (IC) engines are an extremely important equipment. Compression ignition (CI) engines are the most powerful and capable when compared to spark ignition (SI) engines, especially for off-road power generation, marine applications, and large and medium-sized vehicles on the road [1,2]. CI engines become more and more popular because of their exceptional performance, consistent dependability, long lifespan, increased fuel efficiency, and significantly reduced emissions of carbon dioxide (CO_2), carbon monoxide (CO) and hydrocarbons (HCs) compared to SI engines [3−5]. However, it must be acknowledged that CI engines do encounter challenges such as noisy combustion, elevated NO_x emissions, disruptive vibrations, and the release of harmful smoke when compared to SI engines [1,2].

Nomenclature

A_r – pre-exponential factor
b_r – temperature exponent
$\bar{C}_{p,m}$ – molar constant-pressure specific heat, J/(mol·K)
C_μ – model constant
D – diffusion coefficient
e – internal energy, J
E_r – activation energy, kJ/mol
h_m – species enthalpy, J/mol
$\bar{h}_m$ – molar specific enthalpy, J/(mol·K)
I – initial turbulence intensity
k – total kinetic energy, J
K – conductivity, W/(m·K)
K_{cr} – equilibrium coefficient
le – length scale, m
P – pressure, kPa
Pr – Prandtl number
q_i – rate-of-progress variable
R_u – universal gas constant, J/(mol·K)
S – source term
S_m – source terms of species m
t – time, s
T – temperature, K
u, U – velocity, m/s
$[X_m]$ – molar concentration of species m
Y_m – mass fraction of specie m

Greek symbols

ε – turbulent dissipation, m^2/s^3
μ_t – turbulent viscosity, Pa s
ρ – density, kg/m^3
σ_{ij} – stress tensor, Pa
$\upsilon'_{m,r}$, $\upsilon''_{m,r}$ – stoichiometric coefficients for the reactants
$\dot{\omega}_m$ – production rate of species, 1/s

Subscripts and Superscripts

r – reaction
m – species

Abbreviations and Acronyms

AMR – adaptive mesh refinement
BTDC – before top dead centre
CA – crank angle
CAD – computer-aided design
CFD – computational fluid dynamics
CI – compression ignition
CO – carbon monoxide
CO_2 – carbon dioxide
CNG – compressed natural gas
CSP – computational singular perturbation
EGR – exhaust gas recirculation
HCCI – homogeneous charge compression ignition
HCs – hydrocarbons
IC – internal combustion
IDT – ignition delay time
KH-RT – Kelvin-Helmholtz and Rayleigh-Taylor
LLNL – Lawrence Livermore National Laboratory's
MB-NH – methylbutanoate/n-heptane
PRF – principal reference fuel
QSS – quasi-steady-state
SCR – selective catalytic reduction
SI – spark ignition
TDC – top dead centre

Nevertheless, significant advancements have been made in recent times to address these environmental concerns. Various methods have been developed for the reduction of these polluting gases, including exhaust gas recirculation (EGR) [6,7], optimisation of injection systems [8,9], utilisation of AdBlue in selective catalytic reduction (SCR) techniques [10−13], the management of turbulence and chemistry interaction [14,15], adoption of dual fuel engines [16−18], the introduction of biofuels injections [19−24], and using compressed natural gas (CNG) [25]. These innovative approaches hold immense potential for mitigating the adverse effects associated with CI engines, thereby paving the way for a more refined and sustainable future in automotive technology. The advancement of computational fluid dynamics (CFD) methodology for internal combustion engine design presents a distinctive and formidable challenge compared to traditional experimental approaches, owing to the intricate nature of the physics and mechanics involved. Enhancing our comprehension in this field is imperative in order to unlock innovative solutions, streamline costs, and augment development efficiency. While notable progress has been achieved in various domains such as turbulence, spray and combustion modelling, pre- and post-processing, etc., there are still numerous additional prerequisites to be fulfilled for CFD to truly emerge as a reliable and comprehensive design tool [26,27]. The CONVERGE software [28] is widely used in engine research and is popular among universities that train engineers and researchers. It solves complex equations related to fluid dynamics, taking into account factors like turbulence and chemical reactions. A detailed chemistry extension has also been developed to address the need for reducing emissions from internal combustion engines. This extension allows for more accurate simulation of engine exhaust gases. Three-dimensional conservation equations are successfully solved using CONVERGE CFD, both with and without chemical reactions. The code and its functioning have been thoroughly documented by Richards et al. [28]. In response to the need for reducing polluting emissions from internal combustion engines, a comprehensive chemistry extension for CONVERGE has been developed. This extension allows for the accurate representation of engine exhaust gas composition, including radicals, NO_x species and soot.

In this context, different numerical studies have been carried out. For instance, a simplified mechanism with 60 species and 237 reactions was used for the spray combustion simulation in the study [29]. Similar to this, Wan Manson and Olsen [30] used the CONVERGE CFD model to study the combustion and emissions of a gas-diesel dual fuel. They used a simplified chemical kinetic mechanism that had 393 reactions for n-heptane, methane, ethane and propane, and 86 species. In a different research, Ra and Reitz [31] used the n-heptane mechanism in conjunction with a reduced mechanism for iso-octane oxidation to

create a principal reference fuel (PRF) mechanism that included 130 reactions and 41 species. Direct injection diesel engines and homogeneous charge compression ignition (HCCI) engines were used in the trials to verify the PRF mechanism.

Wang and Frenklach [32] employed a comprehensive mechanism that combined the oxidation chemistry of skeletal n-heptane with the kinetics of aromatic formation in fuel-rich acetylene flames, comprising 117 species and 602 reactions. They validated the combustion simulations through detailed numerical kinetic analysis and by comparison with a reduced mechanism of 60 species and 237 reactions. Liu et al. [33] applied graph-based reduction techniques to a detailed MB-NH (methylbutanoate/n-heptane) model containing 661 species and 3019 reactions, producing a reduced mechanism with 145 species and 869 reactions. Combustion simulations performed in CONVERGE software using this reduced chemistry showed good agreement with experimental data for biodiesel blends, indicating the model's suitability for predicting combustion behaviour and emissions trends in compression-ignition engines. Liu and Zhang [34] (2023) developed a reduced diesel mechanism derived from Wang's 2015 mechanism (109 species, 543 reactions) [35]. They first defined an importance index using computational singular perturbation (CSP) to identify and remove insignificant reactions. By applying a threshold of 0.0065, they eliminated 140 reactions, reducing the mechanism to 403 reactions. Using a 0.005 threshold, they also identified 32 global quasi-steady-state (QSS) species. The final reduced mechanism contains 77 species and, when compared with Wang's original mechanism, shows a maximum deviation of 7.2% in ignition delay. They further validated the mechanism by simulating an HCCI engine case and found that the simulation results agree closely with the original mechanism, with errors under 10%.

Yin et al. [36] developed a simplified chemical kinetic mechanism for toluene within a gasoline surrogate (toluene, n-heptane, iso-octane). They reduced the original mechanism from 137 species and 633 reactions to 60 species and 234 reactions. The simplified mechanism accurately predicts ignition delay times and laminar flame speeds according to their results.

Hu et al. [37] proposed a four-step global model for moderate and intensive low-oxygen dilution (MILD) oxy-combustion in 2018. They validated it against two detailed mechanisms across three combustion conditions and compared its performance with five other global mechanisms. The results showed that, under MILD, oxy-fuel and MILD oxy-combustion conditions, the proposed model substantially improved predictions of peak and equilibrium concentrations of the main species. However, the global model was validated only against detailed mechanisms for some reaction conditions where no experimental data were available. While the global model reproduced trends similar to the two detailed mechanisms across the three conditions, the absolute species concentration values differed notably among the three approaches.

Baigmohammadi et al. [38] recently developed a detailed mechanism, NUIGMech1.1, to investigate ignition delay times (IDTs) of C1-C2 hydrocarbons over a range of temperatures, pressures and equivalence ratios. NUIGMech1.1 comprises 11 274 elementary reactions and 2746 species. Its accuracy was assessed by comparison with experimental IDT data, and it was found to reproduce the measured IDTs well.

The main objective of this study is to validate the simplified reaction mechanism of a diesel fuel. This mechanism was created by simulating the actual physical properties of the fuel and using the chemical kinetics of n-heptane, consisting of 42 species and 167 reactions. We compared it with the reduced mechanism of 77 species developed by Liu and Zhang [34].

2. Mathematical formulations

Equations describing the conservation of mass, momentum and energy guide the modelling of combustion in diesel engines. The turbulence and the movement of passive scalars and organisms are described by additional equations. The mathematical formulas utilised in CONVERGE are described in this context in [28].

The following represents the compressible equation for species mass transport:

$$\frac{\partial \rho_m}{\partial t} + \frac{\partial u_j \rho_m}{\partial x_j} = \frac{\partial}{\partial x_j}\left(\rho D \frac{\partial Y_m}{\partial x_j}\right) + S_m. \quad (1)$$

The total fluid density equation is obtained by adding the preceding equation for each species:

$$\frac{\partial \rho}{\partial t} + \frac{\partial \rho u_i}{\partial x_j} = S, \quad (2)$$

where $\rho_m = Y_m \cdot \rho$. In the above equations, the velocity is represented by u, density by ρ, species density by ρ_m, mass fraction of species m by Y_m, mass diffusion coefficient by D, and source terms by S and S_m.

Hence, the following is the equation of momentum transport for the compressible fluid:

$$\frac{\partial \rho u_i}{\partial t} + \frac{\partial u_i u_j}{\partial x_j} = -\frac{\partial P}{\partial x_i} + \frac{\partial \sigma_{ij}}{\partial x_j} + S_i. \quad (3)$$

The energy equation for the compressible fluid is given by:

$$\frac{\partial \rho e}{\partial t} + \frac{\partial u_j \rho e}{\partial x_j} = -P\frac{\partial u_j}{\partial x_i} + \sigma_{ij}\frac{\partial u_i}{\partial x_j} + \frac{\partial}{\partial x_j}\left(K\frac{\partial T}{\partial x_j}\right) + \\ + \frac{\partial}{\partial x_j}\left(\rho D \sum_m h_m \frac{\partial Y_m}{\partial x_j}\right) + S. \quad (4)$$

In the above equations, P is the pressure, T is the temperature, σ_{ij} is the stress tensor, S_i and S are source terms, h_m is the species enthalpy, K is the conductivity, D is the diffusivity, and e is the specific internal energy.

The conductivity is substituted with the turbulent conductivity provided by:

$$K_t = K + c_p \frac{\mu_t}{\mathrm{Pr}}. \quad (5)$$

where Pr and μ_t are the Prandtl number and turbulent viscosity, respectively.

In the initial stages of the pressure-implicit with splitting of operators (PISO) loop, CONVERGE computes the momentum and pressure to determine the velocity for the other transport equations. It is essential to verify the PISO loop convergence after each iteration of the PISO process.

3. SAGE chemical kinetics model

The following section discusses the incorporation of the SAGE model within the CONVERGE software, specifically focusing on chemistry modelling. The inclusion of the SAGE model allows for the integration of detailed chemical kinetics in combustion applications. This is accomplished by using a collection of input files in the CHEMKIN format, which is now the accepted format for describing chemical mechanisms in this context.

A mechanism for a multi-step chemical reaction may be expressed as follows [28]:

$$\sum_{m=1}^{M} \upsilon'_{m,r} x_m \Leftrightarrow \sum_{m=1}^{M} \upsilon''_{m,r}\, x_m, \quad \text{for } r = 1,2,\dots,R. \tag{6}$$

For species m and reaction r, the stoichiometric coefficients for the reactants and products are denoted by $\upsilon'_{m,r}$ and $\upsilon''_{m,r}$, respectively. The chemical symbol for species m is represented by x_m. The following provides the production rate of species m:

$$\dot{\omega}_m = \sum_{r=1}^{R} \upsilon_{m,r}\, q_r\,, \quad \text{for } m = 1,2,\dots,M,$$

$$\upsilon_{m,r} = \upsilon''_{m,r} - \upsilon'_{m,r}, \tag{7}$$

and the rate-of-progress variable q_i for the r^{th} reaction is:

$$q_r = k_{fr} \prod_{m=1}^{M} [X_m]^{\upsilon'_{m,r}} - k_{rr} \prod_{m=1}^{M} [X_m]^{\upsilon''_{m,r}}, \tag{8}$$

where k_{fr} and k_{rr} are the forward and reverse rate coefficients for reaction r, and $[X_m]$ is the molar concentration of species m.

The Arrhenius form is used in the SAGE setup to represent the forward rate coefficient:

$$k_{fr} = A_r T^{b_r} e^{(-E_r/R_u T)}, \tag{9}$$

where R_u is the universal gas constant, E_r is the activation energy, b_r is the temperature exponent, and A_r is the pre-exponential factor.

Additionally, the reverse rate coefficient can be computed using the equilibrium coefficient K_{cr}, or it can be supplied in an equivalent mode:

$$k_{rr} = k_{fr}/K_{cr}. \tag{10}$$

The thermodynamic characteristics are used to calculate the equilibrium coefficient, K_{cr}.

The governing equations for mass and energy conservation for a particular computational cell may be solved using the information provided. These are the equations:

$$\frac{d[X_m]}{dt} = \dot{\omega}_m \quad \text{and} \quad \frac{dT}{dt} = \frac{V\frac{dP}{dt} - \sum_m (\bar{h}_m \dot{\omega}_m)}{\sum_m ([X_m]\bar{C}_{p,m})}, \tag{11}$$

where the molar specific enthalpy, molar constant-pressure specific heat, volume, temperature and pressure of species m are represented by the variables $\bar{h}_m$, $\bar{C}_{p,m}$, V, T and P, respectively. In CONVERGE, the mech.dat and therm.dat data files define the mechanisms and thermodynamic data for the SAGE model input parameters. Every computational time step in the CONVERGE program solves the aforementioned equations, and the species are updated appropriately. Please note that the temperature acquired is not utilised to update the cell temperature in CONVERGE, but solely to update the rate coefficients in the SAGE system of rate equations. After applying the determined species concentrations to converge the thorough chemistry computation, the cell temperature is updated.

4. Engine description and computational domain

The model of the combustion chamber was initially created using SOLIDWORKS, a computer-aided design (CAD) software, before being exported to the preprocessing software CONVERGE CFD for geometry verification and clean-up. Figure 1 illustrates the combustion chamber model generated with Tecplot Graphic. The engine used in our work is a heavy-duty, 6-cylinder, 4-stroke diesel engine with a piston cylinder bow, model number: MK DIR 620-145 whose parameters are gathered in Table 1. It is equipped with a high-pressure injector pump system and a turbocharging system. The simulations run at 1400 rpm, 50% load, and the injection begins at 8° before TDC.

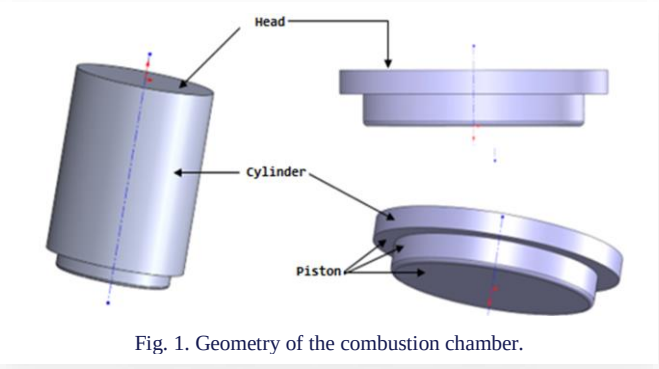

Fig. 1. Geometry of the combustion chamber.

Specifications for the engine combustion chamber and injectors are listed in Table 1. Table 2 enumerates the critical injection requirements, and Fig. 2 depicts the injection profile.

Table 1. Engine specifications.

Engine type	MKDIR 620-145
Chamber type	Vertical valve
Number of cylinders	06
Bore	12 cm
Stroke	14.5 cm
Connecting rod length	22.7 cm
Squish	0.17 cm
Compression ratio	17
Engine speed	1400 rpm
Maximum torque	158 N m at 1200 rpm
Turbocharger	Schwitzer type S2BV
Injection pump	Bosch type P.7100
EGR	0%
Swirl	3.11

Table 2 Injection specification.

Fuel type	n-heptane
Initial fuel temperature	344 K
Injection duration	21°
Fuel Injection rate	0.09 g/cycle
Injection start	8 c.a. degree BTDC
Nozzle diameter	2.59e-01 mm
Nozzles number	2

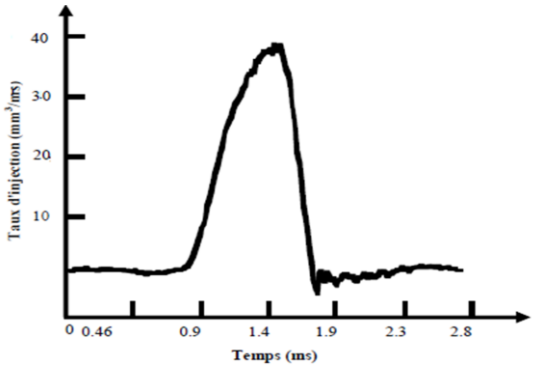

Fig. 2. Injection profile.

In the present work, the detailed boundary conditions (temperature of cylinder, head and piston), and initial conditions (pressure and temperature in the chamber) used in the software are:

- the boundary conditions:

T_{cy} = 433K,
T_{head} = 523 K,
T_p = 523 K,

- the initial conditions:

P_{ch} = 1.765 MPa,
T_{ch} = 355 K.

The process of generating a complex geometry grid in different CFD codes can be quite time-consuming for users, which makes projects unfeasible due to financial or time constraints. The code CONVERGE CFD allows the calculation of three-dimensional, compressible, chemically-reacting fluid flows in complex geometries with moving boundaries, and it is specifically tailored for piston engine analysis. In this study, we used two techniques: basic meshing and the adaptive mesh refinement (AMR) technique to manage and refine the grid for temperature, emissions, and velocity.

The effects of the base grid size in all directions (4 mm, 2.5 mm, 1.8 mm and 1.5 mm) on the combustion are shown in Table 3. AMR was adopted based on the temperature, velocity and near nozzle region cell size of 0.2 mm. According to the mesh sensitivity study, in each of the three dimensions, the base grid size was maintained at 1.8 mm with an error in cylinder pressure of no more than 4.7%.

Table 3. Mesh details.

Base grid size [mm]	AMR [mm]	Error [%]
4	0.2	7.8
2.5	0.2	5.6
1.8	0.2	4.7
1.5	0.2	4.4

A 1.8 mm base grid was applied throughout the computational domain. Owing to piston motion, the total number of computational cells varied over the engine cycle, reaching approximately 589 133 cells at the bottom dead centre (BDC, 180 CA) and decreasing to about 10 154 cells at the top dead centre (TDC, 0 CA). Figure 3 presents the comparison of cylinder pressure from the experiment and simulation, whereas the mesh of the engine domain is illustrated in Fig. 4.

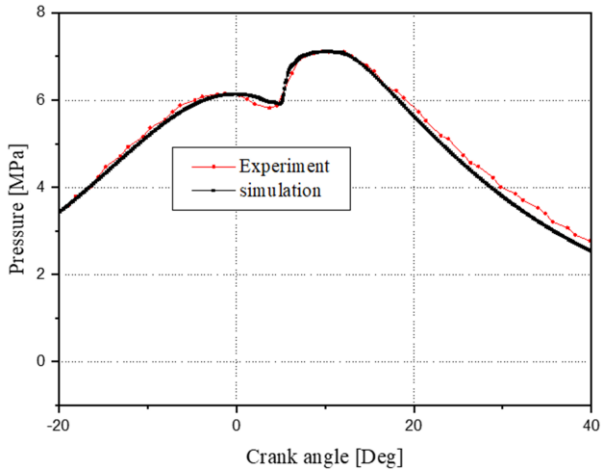

Fig. 3. Experimental and simulated evolution of cylinder pressure.

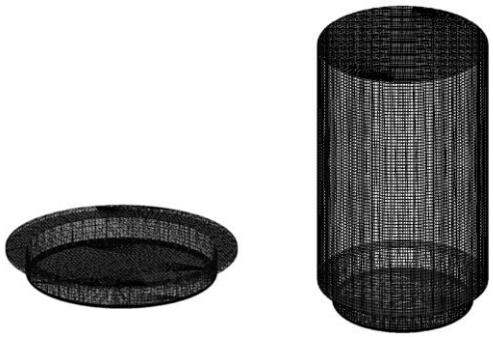

Fig. 4. Computational domain of the engine.

5. Reduced chemical kinetic reaction mechanism

N-heptane is often chosen as a fuel because it has a cetane number of around 56, which is comparable to that of conventional diesel fuel. Heptyl radicals, C_7H_{15}, formed from n-heptane through H-abstraction from fuel molecules, play a significant role in the oxidation process. It is crucial to accurately account for the number of carbon and hydrogen atoms in the final combustion products when calculating the overall heat release of oxidation reactions. Therefore, it is necessary for the simplified reaction mechanism to align with the overall chemical equilibrium state.

In this study, a reduced reaction mechanism comprising 167 chemical reactions and 42 species was considered. For a more detailed mechanism, we recommend consulting the website of the Lawrence Livermore National Laboratory (LLNL), specifically the archived mechanisms available through the U.S. Department of Energy National Nuclear Security Administration (LLNL website). Table 4 provides an excerpt of the n-heptane reaction mechanism. Additional information on reaction mechanisms can be found on the same website. Moreover, alternative literature sources offer other n-heptane mechanisms, such as a comprehensive mechanism with 544 species and 2446 reactions (LLNL), a detailed mechanism with 117 species and

602 reactions, and a reduced mechanism with 60 species and 237 reactions [35].

Table 4. Single column table example.

Reaction		A_r	b_r	E_r
R1	$C_7H_{16} + H = C_7H_{15}{-}1 + H_2$	5.600e+07	2.0	7667.0
R2	$C_7H_{16} + H = C_7H_{15}{-}2 + H_2$	4.380e+07	2.0	4750.0
R3	$C_7H_{16} + OH = C_7H_{15}{-}1 + H_2O$	8.610e+09	1.1	1815.0
...	...	...	...	....
R6	$C_7H_{16} + HO_2 = C_7H_{15}{-}2 + H_2O_2$	1.650e+13	0.0	16950.0
R7	$C_7H_{16} + O_2 = C_7H_{15}{-}1 + HO_2$	2.500e+13	0.0	48810.0
...	...	.....	...	....
R9	C_7H_{15}-1 + $O_2 = C_7H_{15}O_2$	2.000e+12	0.0	0.0
R10	C_7H_{15}-2 + $O_2 = C_7H_{15}O_2$	2.000e+12	0.0	0.0
R11	$C_7H_{15}O_2 = C_7H_{14}O_2H$	6.000e+11	0.0	20380.0
R12	$C_7H_{14}O_2H + O_2 = C_7H_{14}O_2HO_2$	4.600e+11	0.0	0.0
R13–R158	...	...	...	...
R159	$C_2H_3 + H = C_2H_2 + H_2$	4.000e+13	0.0	0.0
R160	$C_2H_3 + O_2 = CH_2O + HCO$	4.000e+12	0.0	–250.0
R161	$C_2H_3 + OH = C_2H_2 + H_2O$	3.000e+13	0.0	0.0
R162	$C_2H_3 + CH_2 = C_2H_2 + CH_3$	3.000e+13	0.0	0.0
...	...	...	...	...
R165	$C_2H_3 + O = C_2H_2 + OH$	1.000e+13	0.0	0.0
R166	$C_2H_2 + OH = CH_3 + CO$	4.830e-04	4.0	–2000.0
R167	$C_2H_3 = C_2H_2 + H$	4.600e+40	–8.8	46200.0

6. Validation of numerical results

The CONVERGE CFD code was utilised to simultaneously predict the combustion process and emissions evolution using specific sub-models: SAGE for combustion, KH-RT (Kelvin-Helmholtz Rayleigh-Taylor hybrid model) for spray, RNG k–ε for turbulence, and the Hiroyasu and Zeldovich models for soot and NO_x emissions, respectively (Richards et al. [28]).

For this study, the re-normalization group (RNG) Reynolds averaged Navier-Stokes (RANS) approach was selected. The total kinetic energy is expressed as $k = 3/2{\cdot}(UI)^2$, where U represents the velocity and I is the initial turbulence intensity (5%). Turbulent dissipation is given by $\varepsilon = C_\mu^{3/4} k^{3/2} le^{-1}$, where ϵ is the turbulent dissipation, C_μ is a model constant, and le is the length scale. The CFD models utilised in the various physical phenomena employ model constants recommended by CONVERGE (Richards et al. [28]).

6.1. Combustion and emissions characteristics

In-cylinder pressure is the primary parameter influencing combustion processes. To validate our chosen reaction mechanism, we compared our cylinder pressure results (using a mechanism of 42 species and 167 reactions) with those of Liu and Zhang [34], who developed a reduced 77-species mechanism for diesel derived from Wang's mechanism (109 species and 543 reactions). Figure 5 illustrates a strong agreement between the numerical and experimental results, which leads to the assumption that results predicted by computational analysis are considerably similar to the actual result by experimental testing. The motoring pressures for both cases rise in a similar manner. However, at TDC, the simulated pressure drops slightly, then increases markedly at 5° after top dead centre (ATDC) due to fuel injection. After 11° TDC, the pressure begins to decline. In contrast, Fig. 6 exhibits a low error margin of 7.2%, confirming the superior accuracy of the present model. The predicted heat release rate is similarly presented in Figure 5.Two distinct phases appear: an initial, rapid heat release from premixed combustion, which peaks at about 350 J/CA around 6° ATDC and can produce high temperatures, followed by a gradual decline into the slower, mixing-controlled diffusion combustion phase.

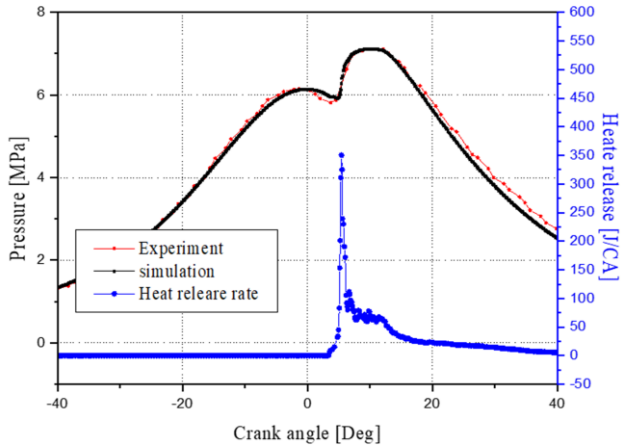

Fig. 5. The cylinder pressure (experimental vs. calculated) and heat release rate evolution.

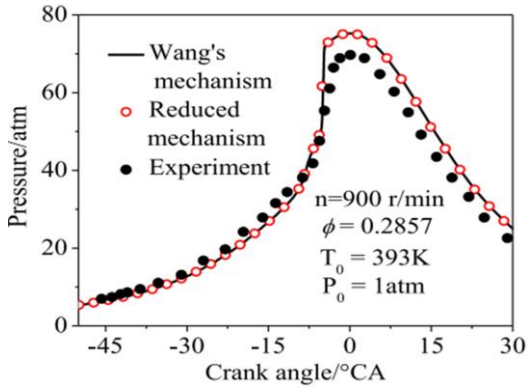

Fig. 6. The cylinder pressure reported by Liu and Zhang (2023) [34].

Figure 7 illustrates the changes in the average cylinder temperature and concentrations of CO, OH and H_2O_2. It is important to note that these species occur at temperatures around 930 K. Likewise, this temperature marks the point at which the concentration of H_2O_2 is sufficient to initiate auto-ignition, coinciding with the maximum heat release rate. Regarding the concentrations of OH and CO, it is clear that high levels of these species occur at the maximum temperature (around 1300K). Figure 8 shows the temporal evolution of n-heptane mass and soot emissions. Soot formation begins simultaneously with soot oxidation immediately after the start of injection (SOI) at 5° ATDC. Dur-

ing the initial stage, the soot formation rate increases, causing the net soot mass to rise until it reaches a maximum of 3.25×10^{-7} kg at 18° ATDC. Thereafter, the soot formation rate decreases, and the net soot mass falls to a final value of 9×10^{-8} kg at the end of the simulation.

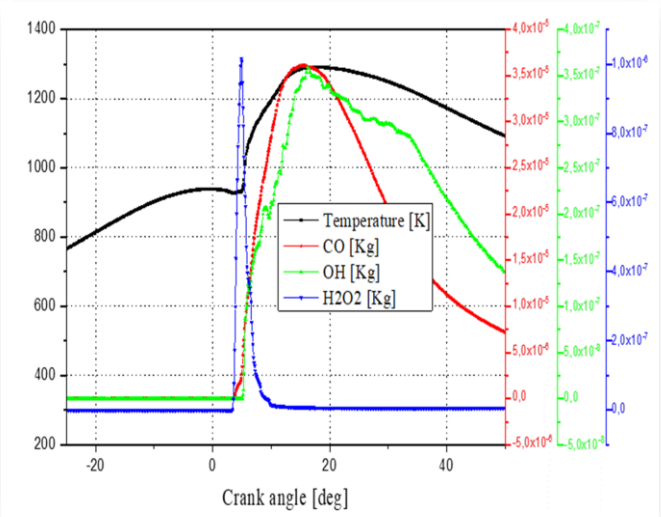

Fig. 7. Evolution of in-cylinder temperature and concentrations of CO, OH and H_2O_2.

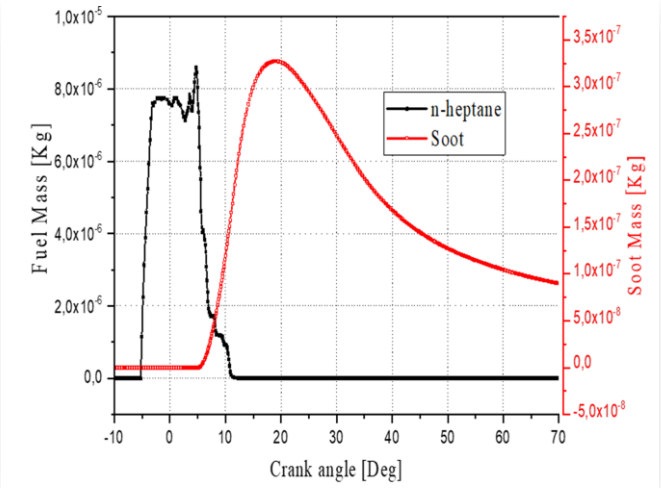

Fig. 8. Evolution of in-cylinder fuel mass and soot emission.

In Fig. 9, the variations in fuel mass, O_2, CO_2, H_2O and HC concentrations are displayed. It is evident that the simulation accurately predicts the concentrations of these species in the combustion products. There is a significant increase in species CO_2, H_2O and HC concentrations during the combustion phase, a contrary to a decrease in O_2. It is clear that the CO_2 and H_2O concentrations rise rapidly during the premixed phase and continue to increase, albeit at a slower rate, during the diffusion phase.

Figure 10 depicts the changes in N_2, NO and NO_x concentrations. It is clearly observed that the concentrations of NO and NO_x increase during the rapid premixed phase of combustion and follow the temperature evolution, reach saturation for NO_x (around 1.1×10^{-4} kg), and decrease for NO during the diffusion phase.

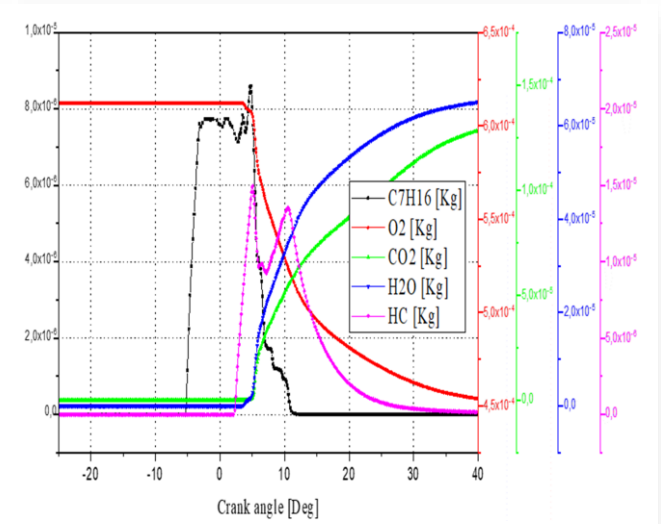

Fig. 9. Evolution of in-cylinder fuel mass and concentrations of O_2, CO_2, H_2O and HC.

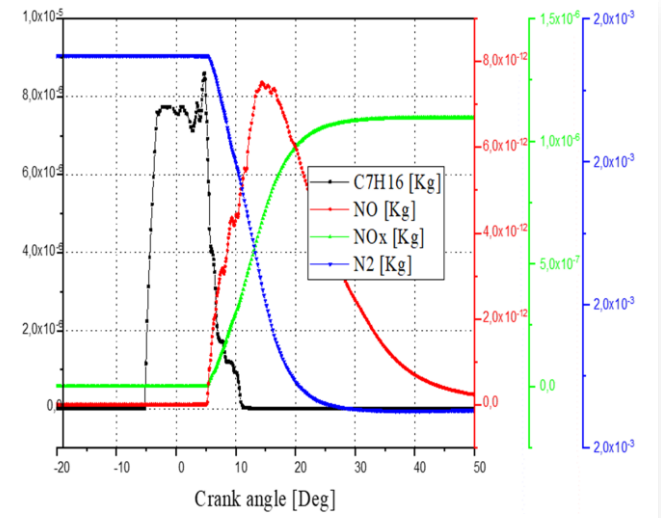

Fig. 10. Evolution of in-cylinder fuel mass and concentrations of NO, N_2 and NO_x.

6.2. Scalar fields

Here, we present the combustion chamber's contours, explain the injection behaviour throughout the cycle, and offer a close-up of the inside to completely depict the results of the numerical simulation. Various crank angles were used to display the temperature distribution and spray progression.

Spray evolution

Figure 11 displays the contours of the fuel spray, indicating that the core of the cold jet contains an excessive amount of fuel. It clearly demonstrates the progression of the diesel spray.

Temperature evolution

The CONVERGE code has successfully predicted the temperature contours in diesel engines at different positions of the crank angle. This can be observed in Fig. 12, where a selection of different crank angles has been chosen to showcase the progression

of the combustion process. By utilising scalar fields, the evolution of the flame is visually represented through the contours of the temperature, and the rich region behaviour is presented by red and green contours. These contours demonstrate that the core of the cold jet contains an excessive amount of fuel, while the actual flame occurs in the space between the jet and the surrounding air (known as a diffusion flame). It is clearly shown that the rich region is identified mostly at the piston bowl wall and near the cylinder head. The temperature contours are observed by slicing through the axis of the spray. Notably, the red contours highlight the presence of a non-premixed flame. It is worth mentioning that the maximum temperature reached is approximately 2500 K. For this reason, it is expected that the formation of NO_x is high in these regions.

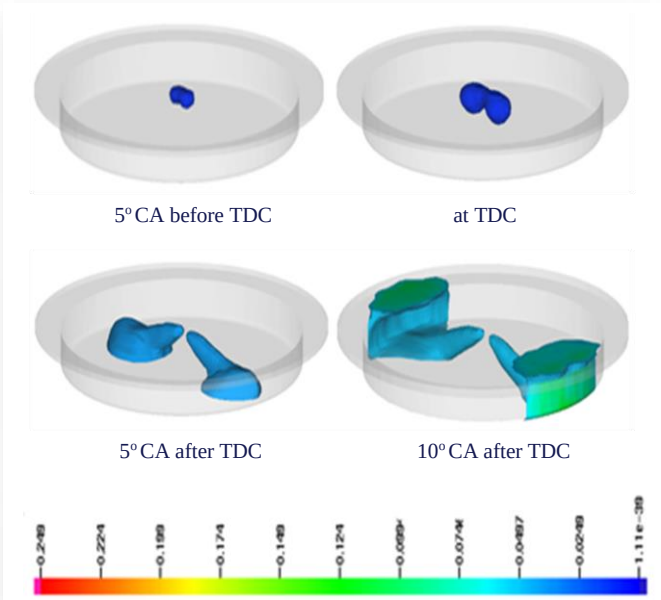

Fig. 11. Spray contours for different angles.

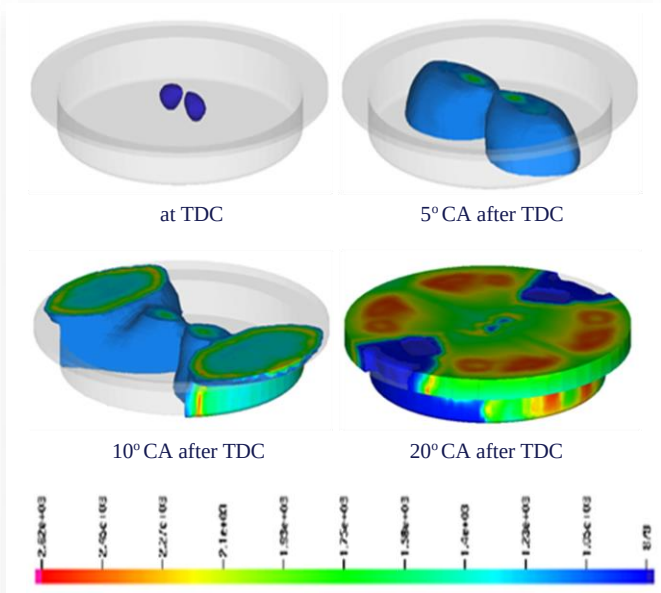

Fig. 12. Temperature distribution for different angles.

7. Conclusions

The combustion and emissions characteristics of a direct injection diesel engine fuelled with n-heptane were investigated using numerical simulations with CONVERGE CFD. The combustion process of n-heptane was analysed using a reduced reaction mechanism comprising 167 chemical reactions and 42 species, and the results were compared with the reduced mechanism developed by Liu and Zhang (2023), which contains 77 species. The main conclusions are summarised as follows:

- According to the results obtained, the combustion model used gives a good estimate of the average pressure in the cylinder – 4.7%, and the distribution of all the species of the reactive mixture can be perfectly described during the combustion phase.
- The heat release rate at its maximum is 350 J/CA at 6 BTDC.
- The concentrations of chemical species such as CO, NO, OH, N_2, HC and soot, unlike those of H_2O, CO_2 and NO_x, seem adjusted by dosage and decrease rapidly during the slow diffusion phase of combustion.
- These species appear at temperatures of about 930 K, where the concentration of H_2O_2 is sufficient to initiate autoignition, and high levels of OH and CO are observed at a temperature of 1300 K.
- The evolution of the H_2O_2 concentrations seems to be related to that of the peaks of the in-cylinder pressure and average temperature in the cylinder during the premixed combustion phase.
- The simulation results indicate that soot is produced at the beginning of the combustion process by diffusion (around 18° BTDC, with a maximum value of 3.25×10^{-7} kg).
- The evolution of NO_x follows the evolution of temperature, reaching saturation at about 1.1×10^{-4} kg.
- During the combustion phase, we observe an increase in CO_2, H_2O and HC species; on the other hand, O_2 decreases.
- The simulation results indicate that the diesel fuel model, which accounts for the n-heptane reaction mechanism and physical properties, possesses sufficient accuracy for implementation in more advanced computations.
- The model validated in this research will be utilised to develop fuel and biofuel injection strategies aimed at reducing emissions.
- The logic progression of this research will involve the development of a CFD model for engines that includes soot prediction capabilities, as well as engine experiments using n-heptane blended with alcohols (ethanol, methanol and MTBE) under mixing conditions. This will test the capabilities of the CFD model in the complex environment inside an engine and enhance our understanding of the pollution formation tendencies in heavy-duty engines.

Acknowledgements

The authors would like to thank Ecole Nationale Polytechnique d'Oran, LTE Laboratory, Department of Mechanical Engineering, ENP MA-Oran, Algeria. The authors would also like to

thank the CONVERGE CFD for their support throughout the research work.

References

[1] Heywood, J.B. (1983). *Internal Combustion Engine Fundamentals*. New York, McGraw-Hill Inc.

[2] Ramos, J.I. (1989). *Internal Combustion Engine Modeling*. Hemisphere Publishing Corporation.

[3] Baumgarten, C. (2006). *Mixture Formation in Internal Combustion Engines*. Springer-Verlag Berlin Heidelberg, New York.

[4] De Risi, A., Donateo, T., & Laforgia, D. (2020). Theoretical investigation on the influence of physical parameters on soot and NO_x engine emissions. *Proceedings of the ASME 2001 Internal Combustion Engine Division Spring Technical Conference*. 2001ICES2001-120, 53−64, April 29–May 2, Philadelphia, Pennsylvania, USA. doi: 10.1115/ICES2001-120

[5] Bousbaa, H., Liazid, A., Sary, A., & Tazerout, M. (2013). Numerical Investigations on the use of Waste Animal Fats as fuel on DI Diesel engine. *Journal of Petroleum Technology and Alternative Fuels*, 4(7), 131−142. doi: 10.5897/JPTAF2013.0096

[6] Zu, X-H., Yang, C-L., Wang, H-C., & Wang, Y-Y. (2019). Experimental study on diesel engine exhaust gas recirculation performance and optimum exhaust gas recirculation rate determination method. *Royal Society Open Science*, 6(6), 181907. doi: 10.1098/rsos.181907

[7] De Serio, D., De Oliveira, A., & Sodré, J.R. (2017). Effects of EGR rate on performance and emissions of a diesel power generator fueled by B7. *Journal of Brazilian Society of Mechanical Sciences and Engineering*, 39, 1919−1927. doi: 10.1007/s40430-017-0777-x

[8] Fayad, M.A. (2019). Effect of fuel injection strategy on combustion performance and NO_x/smoke trade-off under a range of operating conditions for a heavy-duty DI diesel engine, *SN Applied Sciences*, 1, 1088. doi: 10.1007/s42452-019-1083-2

[9] Medjahed, L., & Bousbaa, H. (2021). Effect of injection parameters on combustion and emissions characteristics of a Turbocharged DI diesel engine. A CFD approach using CONVERGE. *The First International Conference on Energy Transition and Security ICETS'21*, 22−24 May, Adrar, Algeria.

[10] Timpanaro, A. (2019). *Reduction of NO_x Emissions in a Single Cylinder Diesel Engine Using SNCR with In-Cylinder Injection of Aqueous Urea Using SNCR with In-Cylinder Injection of Aqueous Urea*. UNF Graduate Theses, University of North Florida.

[11] Demir, U., Kozan, A., & Özer, S. (2022). Experimental investigation of the effect of urea addition to fuel on engine performance and emissions in diesel engines. *Fuel*, 311, 122578. doi: 10.1016/j.fuel.2021.122578

[12] Spoof-Tuomi, K., Niemi, S., Ovaska, T., Nilsson, O., & Heikkilä, S. (2021). Selective Catalytic Reduction on Filter Performance Testing on Non-road Diesel Engine. *SAE Technical Paper*, 2021-01-5054. doi: 10.4271/2021-01-5054

[13] Gurusamy, P.K., Gandhi, U., Mangalanathan, U., & Lr, K.M. (2017). Measurement of diesel exhaust fluid concentration in urea-SCR after-treatment system. *International Journal of Precision Engineering and Manufacturing*, 18(8), 1085−1092. doi: 10.1007/s12541-017-0127-z

[14] Zhou, Q., Lucchini, T., D'Errico, G., & Hardy, G. (2019). Validation of Diesel Combustion Models with Turbulence Chemistry Interaction and Detailed Kinetics, *SAE Technical Paper*, 2019-24-0088. doi: 10.4271/2019-24-0088

[15] Mohan, R.V., & Haworth, D.C. (2015). Turbulence-chemistry interactions in a heavy-duty compression-ignition engine. *Science Direct*, 35(3), 3053−3060. doi: 10.1016/j.proci.2014.06.098

[16] Chen, Z., Zhang, T., Wang, X., Chen, H., Geng, L., & Zhang, T. (2021). A comparative study of combustion performance and emissions of dual-fuel engines fueled with natural gas/methanol and natural gas/gasoline. *Energy*, 237, 121586. doi: 10.1016/j.energy.2021.121586

[17] Qin, Z., Yang, Z., & Jia, C. (2020). Experimental study on combustion characteristics of diesel–hydrogen dual-fuel engine. *Journal of Thermal Analysis and Calorimetry*, 142, 1483–1491. doi: 10.1007/s10973-019-09147-y

[18] Han, J., Somers, L.M.T, Cracknell, R., Joedicke, A., Wardle, R., & Mohan, V.R.R. (2020). Experimental investigation of ethanol/diesel dual-fuel combustion in a heavy-duty diesel engine. *Fuel*, 275, 117867. doi: 10.1016/j.fuel.2020.117867

[19] Bousbaa, H., Tarabet, L., Khatir, N., & Liazid, A. (2020). Numerical Study on a Diesel Engine fueled by Eucalyptus biofuel using CONVERGE CFD Software. *Journal of Sciences and Technology*, 2(1), 106−119.

[20] Bousbaa, H., Tarabet, L., Naima, K., Liazid, A., & Tazerout, M. (2019). Eucalyptus Biofuel Study as Alternative for Diesel Engine, *International Journal of Renewable Energy Technology*, 10(3), 247–281. doi: 10.1504/IJRET.2019.10022907

[21] Naima, K., Bousbaa, H., Tarabet, L., Menni, Y., & Lorenzini G. (2022). A Comparative Assessment of Combustion Behavior and Emissions Characteristics of DI Diesel Engine Fueled with Waste Plastic Oil and Eucalyptus Biofuel for Sustainable Development Applications. *International Journal of Low-Carbon Technologies*, 17, 1399–1405. doi: 10.1093/ijlct/ctac114

[22] Elkelawy, M. Bastawissi, H.A.E., El Shenawy, E.A., Shams, M.M., Panchal, H., Sadasivuni, K.K., & Choudhary, A.K. (2021). Influence of lean premixed ratio of PCCI-DI engine fueled by diesel/biodiesel blends on combustion, performance, and emission attributes; a comparison study. *Energy Conversion and Management: X*, 10, 100066. doi: 10.1016/j.ecmx.2020.100066

[23] Singh, A.K., Pali, H.S., & Khan, M.M. (2024). Experimental Investigations of CI Engine Performance using Ternary Blends of n-Butanol/Biodiesel/Diesel and n-Octanol/Biodiesel/Diesel. *Archives of Thermodynamics*, 45(1), 109−118. doi: 10.24425/ather.2024.150443

[24] Kumar, D., Kumar, N., & Chaudhary, R. (2024). Use of butanol, pentanol and diesel in a compression ignition engine: A review. *Archives of Thermodynamics*, 45(4), 27−35. doi: 10.24425/ather.2024.151994

[25] Neeraj, K., Arora, B.B., & Maji, S. (2023). Environmental impact evaluation of diesel engine fuelled with CNG. *Archives of Environmental Protection*, 49(1), 79–84. doi: 10.24425/aep.2023.144740

[26] Bousbaa, H., & Bouhadja, Y. (2019). Numerical study of the combustion process and emissions pollution in a spark ignition engine. *Communication Science and Technology*, 21, 41−58.

[27] Bousbaa, H., Benayad, Z., & Naima, K. (2022). Numerical Analysis of Fuels Type Effect on Combustion and Emissions of Turbo-Charged Direct Injection Engine. *Energy and Thermofluids Engineering*, 2, 31–38. doi: 10.38208/ete.v2.531

[28] Richards, K.J., Senecal, P.K., & Pomraning, E. (2022). *CONVERGE 2.1.0, Theory Manual A Three-Dimensional Computational Fluid Dynamics Program for Transient or Steady-State Flow with Complex Geometries*, Convergent Science, Inc.

[29] Rente, T., Golovitchev, V.I., & Denbratt, I. (2001). Numerical Study of n-Heptane Spray Auto-Ignition at Different Levels of Pre-Ignition Turbulence. *The Fifth International Symposium on Diagnostics and Modeling of Combustion in Internal Combustion Engines (COMODIA 2001)*, pp. 86−91, July 1−4, Nagoya, Japan.

[30] Wan Mansor, W.N., & Olsen, D.B. (2016), Computational Modeling of Diesel and Dual Fuel Combustion Using Converge CFD Software, *ARPN Journal of Engineering and Applied Sciences*, 11(23), 13697−13707.

[31] Ra, Y., & Reitz, R.D. (2008). A reduced chemical kinetic model for IC engine combustion simulations with primary reference fuels. *Combustion and Flame*, 155(4), 713–738. doi: 10.1016/j.combustflame.2008.05.002

[32] Wang, H., & Frenklach, M. (1997), A detailed kinetic modeling study of aromatics formation in laminar premixed acetylene and ethylene flames. *Combustion and Flame*, 110(1−2), 173−221. doi: 10.1016/S0010-2180(97)00068-0

[33] Liu, W., Sivaramakrishnan, R., Davis, M.J., Som, S., Longman, D.E., & Lu, T.F. (2013). Development of a reduced biodiesel surrogate model for compression ignition engine modeling. *Proceedings of the Combustion Institute*, 34(1), 401–409. doi: 10.1016/j.proci.2012.05.090

[34] Liu, C., & Zhang, D. (2023). A reduced chemical kinetic mechanism of diesel fuel for HCCI engines. *Journal of Measurements in Engineering*, 11(1). doi: 10.21595/jme.2023.23132

[35] Wang, H., Yao, M., Yue, Z., Jia, M., & Reitz, R.D. (2015). A reduced toluene reference fuel chemical kinetic mechanism for combustion and polycyclic-aromatic hydrocarbon predictions. *Combustion and Flame*, 162(6), 2390–2404. doi: 10.1016/j.combustflame.2015.02.005

[36] Yin, P., Zhang, C., Zhou, A., Li, S., & Li, Y. (2020). A Reduced Chemical Kinetic Mechanism for Toluene, Reference Fuels Based On DRGEP and QSSA Methods. *Technical Gazette (Tehnički vjesnik)*, 27(5), 1571−1578. doi: 10.17559/TV-20190913062824

[37] Hu, F., Li, P., Guo, J., Liu, Z., Wang, L., Mi, J., Dally, B., & Zheng, C. (2018). Global reaction mechanisms for MILD oxy-combustion of methane. *Energy*, 147, 839−857. doi: 10.1016/j.energy.2018.01.089

[38] Baigmohammadi, M., Patel, V., Martinez, S., Panigrahy, S. Ramalingam, A.; Burke, U., Somers, K.P., Heufer, K.A.; Pekalski, A., & Curran, H.J (2020), A Comprehensive Experimental and Simulation Study of Ignition Delay Time Characteristics of Single Fuel C_1-C_2 Hydrocarbons over a Wide Range of Temperatures, Pressures, Equivalence Ratios, and Dilutions. *Energy & Fuels*, 34(3), 3755−3771. doi: 10.1021/acs.energyfuels.9b04139